gomerization would provide a platform for the formation of larger protein complexes.

SAM domain interactions in other proteins are energetically favorable and may therefore mediate the formation of stable complexes in the cell that resemble the polymeric structure described for the EphB2 SAM domain. Indeed, the PcG proteins form large multiprotein complexes. SAM domains from the PcG proteins are relatively promiscuous in their interactions, suggesting that such oligomers could contain a variety of SAM domains. If so, a wide array of binding pockets could be created between SAM domains, multiplying the potential complexity of the surface for specific interactions with other proteins. Though not yet observed, Eph receptors could also form heterogeneous receptor complexes and potentially trigger a wider variety of signaling cascades. It is known that their ligands, the ephrins, can bind to multiple receptor isoforms and could therefore mediate hetero-oligomeric receptor formation (*32*). Similar combinatorial mechanisms are used by other cell surface receptors (*33*).

SAM domains are a diverse family of protein modules involved in many biological processes. As a result, their functional roles may vary and alternate oligomerization mechanisms may be used in different contexts. The EphB2-SAM domain structure described here provides a structural foundation for uncovering the functional roles of this important protein interaction module (*35*).

**References and Notes**


1. M. Tessier-Lavigne, *Cell* **82**, 345 (1995); H. Hirai, Y. Maru, K. Hagiwara, J. Nishida, F. Takaku, *Science* **238**, 1717 (1987).
2. F. Sakane, S. Imai, M. Kai, I. Wada, H. Kanoh, *J. Biol. Chem.* **271**, 8394 (1996).
3. H. Tu, M. Barr, D. Dong, M. Wigler, *Mol. Cell. Biol.* **17**, 5876 (1997).
4. J. Shultz, C. P. Ponting, K. Hoffman, P. Bork, *Protein Sci.* **6**, 249 (1997).
5. C. P. Ponting, *ibid.* **4**, 1928 (1995).
6. M. Kyba and H. Brock, *Dev. Genet.* **22**, 74 (1998).
7. D. Bornemann, E. Miller, J. Simon, *Development* **122**, 1621 (1996).
8. M. Therrien, A. M. Wong, G. M. Rubin, *Cell* **95**, 343 (1998).
9. T. Pawson, *Nature* **373**, 575 (1995); _____ and J. D. Scott, *Science* **278**, 2075 (1997).
10. C. Jousset *et al.*, *EMBO J.* **16**, 69 (1997); T. Golub, G. Barker, M. Lovett, D. Gilliland, *Cell* **77**, 307 (1994).
11. The SAM domain of the ETS family of transcription factors has been called a pointed domain. Kyba and Brock (*6*), however, uncovered a clear sequence relation between the pointed domain and the SAM domain. The relation between the pointed domain and the SAM domain is confirmed by comparison of the EphB2 SAM domain and the structure of the pointed domain from the ETS-1 transcription factor [C. M. Slupsky *et al.*, *Proc. Natl. Acad. Sci. U.S.A.* **95**, 12129 (1998)]. The two structures show a common global folding pattern. There are significant differences in the structures, however, particularly at the $NH_2$-terminus and in the long loop region between the second and the fourth helices of the EphB2-SAM domain.
12. T. Golub *et al.*, *Proc. Natl. Acad. Sci. U.S.A.* **92**, 4917 (1995); M. Carroll, M. Tomasson, G. Barker, T. Golub, D. Gilliland, *ibid.* **93**, 14845 (1196); P. Papadopoulos, S. A. Ridge, C. A. Boucher, C. Stocking, L. M. Wiedemann, *Cancer Res.* **55**, 34 (1995); S. Tosi *et al.*, *Genes Chromosomes Cancer* **21**, 223 (1998).
13. V. Lacronique *et al.*, *Science* **278**, 1309 (1997).
14. A. Peterson *et al.*, *Mol. Cell. Biol.* **17**, 6683 (1997).
15. M. Barr, H. Tu, L. Van Aelst, M. Wigler, *ibid.* **16**, 5597 (1996).
16. C. D. Thanos, C. A. Kim, J. U. Bowie, unpublished results.
17. C. Serra-Pages *et al.*, *EMBO J.* **14**, 2827 (1995).
18. E. Stein *et al.*, *Genes Dev.* **12**, 667 (1998).
19. E. Stein, D. Cerretti, T. Daniel, *J. Biol. Chem.* **271**, 23588 (1996).
20. B. B. Hock *et al.*, *Proc. Natl. Acad. Sci. U.S.A.* **95**, 9779 (1998).
21. H. U. Wang, Z.-F. Chen, D. J. Anderson, *Cell* **93**, 741 (1998); Q. Xu, G. Alldus, R. Macdonald, D. Wilkinson, N. Holder, *Nature* **381**, 319 (1996); H.-J. Cheng, M. Nakamoto, A. D. Bergemann, J. G. Flanagan, *Cell* **82**, 371 (1995).
22. W. Hendrickson, J. Horton, D. LeMaster, *EMBO J.* **9**, 1665 (1990); V. Ramakrishnan, http://snowbird.med.utah.edu/~ramak/madms/segrowth.html
23. A DNA sequence encoding residues 905 to 981 from EphB2 was amplified by polymerase chain reaction from a human renal microvascular endothelial cell cDNA library and subcloned into a modified pet vector optimized for enhanced expression. The vector-encoded sequence Met-Glu-Lys-Thr-Arg was added to the $NH_2$-terminus of the SAM domain so that in our numbering scheme, residue 6 corresponds to residue 905 in the full-length receptor. The protein was purified to homogeneity with anion and cation exchange chromatography and gel-filtration chromatography. The protein was crystallized by hanging drop crystallization at 4°C. The drop contained a 1:1 mixture of reservoir buffer and protein at 20 mg/ml. The reservoir contained 100 mM Hepes (pH 7), 10 mM tris, 20 mM dithiothreitol, 30 mM $Li_2SO_4$, and 26 to 30% Peg 1000.
24. V. Biou and V. Ramakrishnan, *Methods Enzymol.* **276**, 538 (1997).
25. A. T. Brünger, *Nature* **355**, 472 (1992); P. D. Adams, N. S. Pannu, R. J. Read, A. T. Brünger, *Proc. Natl. Acad. Sci. U.S.A.* **94**, 5018 (1997); N. S. Pannu and R. J. Read, *Acta Crystollogr.* **52**, 659 (1996).
26. The conserved residues in the family of SAM domains as defined by Shultz *et al.* (*4*) are all buried within a monomer, with two exceptions. The first exception is Gly[53], which is found in a tight turn between helices 3 and 4. This residue adopts a positive $\phi$ angle and glycine is probably needed to facilitate the otherwise unfavorable backbone conformation. The second exception is Tyr[8] on the $NH_2$-terminal loop. Tyrosine-8 is the key residue in one of the oligomeric interfaces.
27. H. L. De Bondt *et al.*, *Nature* **363**, 595 (1993).
28. J. Janin and F. Rodier, *Proteins Struct. Funct. Genet.* **23**, 580 (1995).
29. D. A. Doyle *et al.*, *Cell* **85**, 1067 (1996).
30. In 31 Eph receptor sequences, Asp[48] is invariant, position 16 is always a negatively charged residue, position 28 is a negatively charged residue in 30 sequences, and position 47 is a negatively charged residue in 29 sequences.
31. C. D. Thanos, M. Phillips, J. U. Bowie, data not shown.
32. N. W. Gale *et al.*, *Neuron* **17**, 9 (1996).
33. E. Ruoslahti and M. D. Pierschbacher, *Science* **238**, 491 (1987); A. Weiss and J. Schlessinger, *Cell* **94**, 277 (1998).
34. R. Miller, S. M. Gallo, H. G. Khalak, C. M. Weeks, *J. Appl. Crystallogr.* **27**, 613 (1994); Z. Otwinowsky, in *Isomorphous Replacement and Anomalous Scattering, Proceedings of the CCP4 Study Weekend*, W. Wolf, P. R. Evans, A. G. W. Leslie, Eds. (SERC Daresbury Laboratory, Warrington, UK, 1991), pp. 80–86; K. D. Cowtan and P. Main, *Acta Crystallogr. D* **52**, 43 (1996); T. A. Jones, J. Y. Zou, S. W. Cowan, M. Kjelgaard, *Acta Crystallogr. A* **47**, 110 (1991); A. T. Brünger *et al.*, *Acta Crystallogr. D* **54**, 905 (1998).
35. P. J. Kraulis, *J. Appl. Crystallogr.* **24**, 946 (1991); R. Koradi *et al.*, *J. Mol. Graphics* **14**, 51 (1996); A. Nicholis *et al.*, *Proteins Struct. Funct. Genet.* **11**, 281 (1991).


36. We thank M. Phillips for performing the sedimentation experiments, T. Daniel for clones and helpful discussions, and D. Eisenberg, T. Yeates, D. Cascio, S. Faham, R. Landgraf, F. Pettit, C. Kim, E. Toth, C. Colovos, E. Marcotte, and M. Saper for advice and comments on the manuscript. Supported by an NSF National Young Investigator and a Pew Scholar Award to J.U.B. and an NIH training grant to C.D.T. This work is dedicated to the memory of Marcia Robb Whitt.

13 November 1998; accepted 29 December 1998


# Single-Channel Recording of a Store-Operated $Ca^{2+}$ Channel in Jurkat T Lymphocytes


**Hubert H. Kerschbaum[1] and Michael D. Cahalan[2]***



**In T lymphocytes, a store-operated calcium ion ($Ca^{2+}$) entry mechanism termed the calcium release–activated $Ca^{2+}$ channel (CRAC channel) underlies the sustained or oscillatory intracellular calcium concentration signal required for interleukin-2 gene expression and cell proliferation. The use of sodium ions as a current carrier enabled single-channel recordings of CRAC channels during activation, inactivation, and blockade of current in the presence of divalent cations. A large conductance of 36 to 40 picosiemens indicates that 100 to 400 CRAC channels are present in T lymphocytes.**


Calcium influx is activated by the depletion of calcium ions from intracellular stores in many electrically inexcitable cells (*1*). In T lymphocytes, a specific type of store-operated channel, the CRAC channel, supports the intracellular calcium concentration signal that leads to lymphocyte activation (*2*). CRAC channels are highly selective for calcium ions under physiological conditions (*3*) and have a tiny single-channel conductance, estimated by fluctuation analysis to be 24 fS in 100 mM extracellular calcium (*4*). This conductance is too low to be resolved at the single-channel


[1]Department of Animal Physiology, Institute of Zoology, University of Salzburg, A-5020 Salzburg, Austria. [2]Department of Physiology and Biophysics, University of California, Irvine, CA 92697, USA.

*To whom correspondence should be addressed. E-mail: mcahalan@uci.edu

level. CRAC channels, like voltage-dependent $Ca^{2+}$ channels, are permeable to monovalent cations (including organic cations up to 6 Å in diameter) when the concentration of extracellular divalent ions is reduced (*5*–*7*).

To detect the activity of single CRAC channels, we lowered the concentration of external divalent cations to the micromolar range to enable $Na^+$ to serve as the charge carrier, eliminated $Mg^{2+}$ from the pipette solution to prevent inactivation of the monovalent current (*7*), and measured current over a range of potentials to –120 mV during whole-cell recording (*8*). CRAC channels were activated either by passive $Ca^{2+}$ store depletion with the $Ca^{2+}$ chelator 1,2-bis(2-aminophenoxy)ethane-*N*,*N*,*N*′,*N*′-tetraacetic acid (BAPTA) or by store depletion in response to added inositol 1,4,5-trisphosphate ($IP_3$). When carrying either $Ca^{2+}$ or $Na^+$ current, CRAC channels opened with a similar biphasic time course during passive store depletion initiated by whole-cell dialysis, but macroscopic whole-cell $Na^+$ currents were typically 40 times as large (Fig. 1, A and B). Current-voltage (*I-V*) relations revealed weak inward rectification of the current with a very positive reversal potential for the $Ca^{2+}$ current and a reversal potential near 0 mV for the $Na^+$ current through CRAC channels (Fig. 1, C and D). The initial activation of $Na^+$ current was composed of discrete current steps, with a succession of identical steps leading to the macroscopic current (Fig. 1E). The steps are multiples of a unitary current of 4.6 pA at –120 mV, corresponding to a conductance of 38 pS. Single-channel currents observed during voltage-ramp stimuli exhibited the same reversal potential and weakly rectifying *I-V* shape as those of the macroscopic current (Fig. 1F). Dialysis with 10 μM $IP_3$ more rapidly elicited the same 36 to 40 pS single-channel activity (*9*).

Single channels at the onset of CRAC channel activation initially exhibited very brief openings before suddenly stabilizing in the open configuration (Fig. 2, A to C). In an examination of 800 data segments (sweeps), each lasting 0.2 s, from 20 cells during which 120 channels began to conduct, the vast majority of single-channel events occurred in equal-sized increments, consistent with unitary increases in the number of conducting channels rather than a gradual increase in their open probability $P_o$ during the activation of CRAC channels. Of thousands of single-channel events, 10 were initially twice the amplitude of the single-channel events because two channels appeared to activate simultaneously within the resolution of the measurement (1 kHz); larger amplitudes were never observed. Brief closures from the open state were voltage-dependent; the duration of these closures increased with depolarization from 3 ± 1 ms at –120 mV to 10 ± 5 ms at –60 mV ($n$ = 3 cells). This voltage dependence may contribute to the inwardly rectifying shape of the *I-V* relation. At –120 mV, $P_o$ was estimated to be 0.94 ± 0.04 ($n$ = 41 sweeps recorded at the time of a single conducting channel in four cells). Longer closures caused fluctuations in the number of conducting channels, but the progressive appearance of new single-channel events led to peak macroscopic currents that varied from 447 to 1539 pA in 45 cells, corresponding to 100 to 360 channels per cell, with an average surface density of 0.36 channels square per/micrometer.

With internal $Mg^{2+}$ present, monovalent current through CRAC channels inactivates slowly over several tens of seconds after the removal of external divalent ions (*5*–*7*). The activation of monovalent CRAC currents occurred with a similar time course with or without internal $Mg^{2+}$ present, and similar single-channel events were observed (Fig. 2, D to F), but current densities were one-tenth those when $Mg^{2+}$ was absent in the pipette solution; this suggested that about 90% of the available CRAC channels were inactivated (*10*). When external divalent cations were removed shortly after the onset of CRAC channel activation, the time course of inactivation was revealed as a progressive closure of single channels (Fig. 3). Evaluated at –120 mV, the initial 40- to 45-pA current represented the activity of eight or nine ion channels, and successive traces showed a stepwise decline in current, finally stabilizing at 4.9 pA, representing the activity of one ion channel. These results demonstrate that changes in the number of conducting channels underlie both the activation and inactivation processes.

We used channel blockers to confirm that

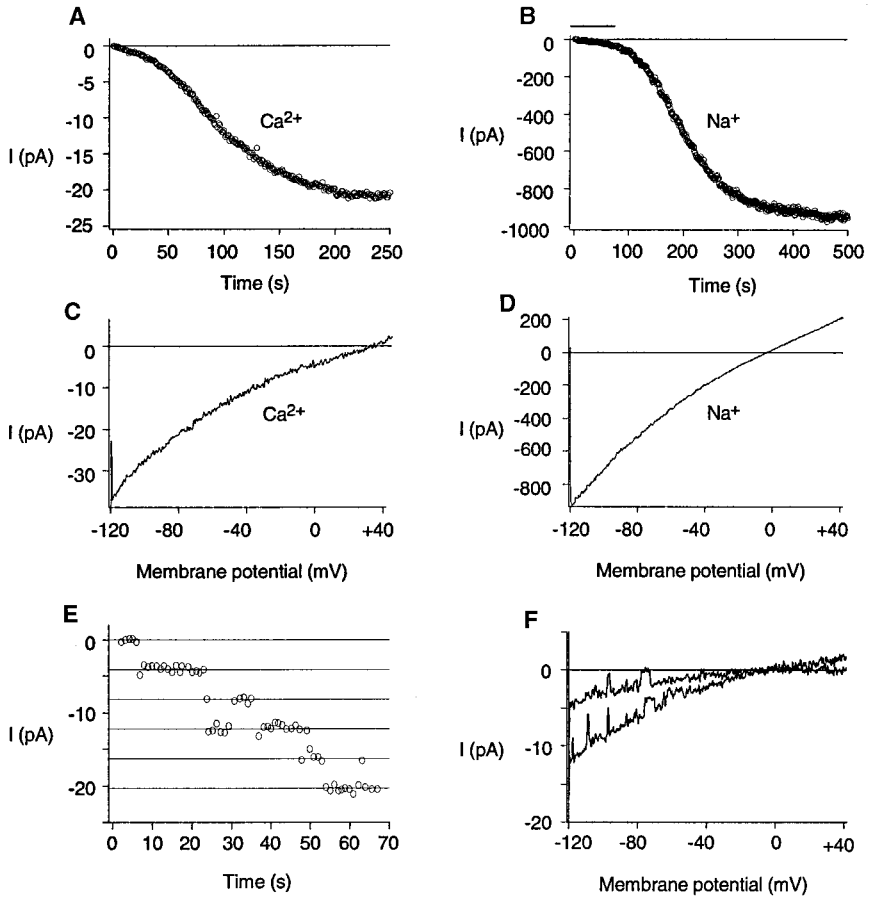


**Fig. 1.** Divalent and monovalent current through a store-operated $Ca^{2+}$ channel in Jurkat cells. (**A**) Activation of $Ca^{2+}$ current through CRAC channels. $Na^+$ methane sulfonate external solution contained 20 mM $Ca^{2+}$; pipette solution was $Mg^{2+}$-free. Voltage ramp stimuli, which increased from –120 to +40 mV in 200 ms, were delivered every second, and the current amplitude at –120 mV during each ramp was plotted at varying times after the initiation of whole-cell recording. (**B**) Activation of $Na^+$ current through CRAC channels. The $Na^+$ methane sulfonate external solution contained HEDTA to chelate inorganic divalent cations; pipette solution was $Mg^{2+}$-free. Voltage ramp stimuli and currents are plotted as in (A). The bar indicates measurements enlarged in (E). (**C**) $Ca^{2+}$ current showing inward rectification. The inward current is carried by $Ca^{2+}$, and the outward current above +40 mV is carried by $Cs^+$. (**D**) $Na^+$ current from the cell shown in (B). Inward current is carried by $Na^+$ and outward current by $Cs^+$. (**E**) Magnification of the first 70 s of the initial phase of current activation. Horizontal lines are multiples of 4.6 pA. (**F**) Current traces during voltage ramps from the cell shown in (B) and (E), showing single-channel activity initially with one channel and later with three ion channels activated.

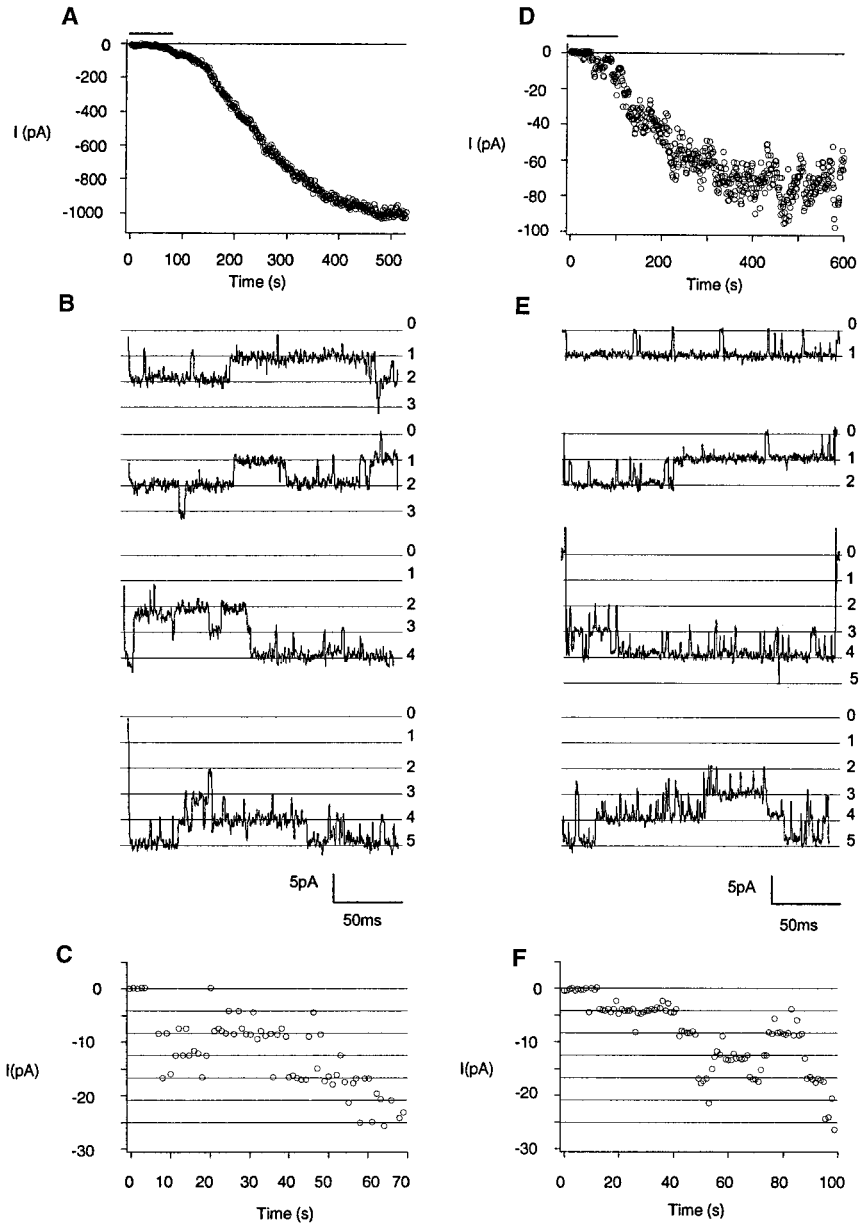


**Fig. 2.** Decreased amplitude of the macroscopic current, but not the single-channel current, in the presence of internal $Mg^{2+}$. CRAC channels were activated by passive depletion of internal stores, and currents during 200-ms voltage steps from 0 to –120 mV were recorded every second. (**A**) HEDTA-containing external solution, $Mg^{2+}$-free pipette solution. The bar indicates measurements enlarged in (C). (**B**) Four current traces showing the activity of one to five ion channels from the cell shown in (A). Lines are equally spaced multiples of 4.3 pA. Numbers to the right indicate the number of open channels. (**C**) Detail of the first 70 s, showing clustering of openings at particular current values from the cell shown in (A). (**D**) Activation of $Na^+$ current with HEDTA-containing external solution and $Mg^{2+}$-containing pipette solution. The bar indicates the first 100 s, shown in greater detail in (F). (**E**) Four current traces from the cell shown in (D), showing the activity of one to five ion channels. (**F**) Detail of (D) illustrating discrete openings at particular current values.

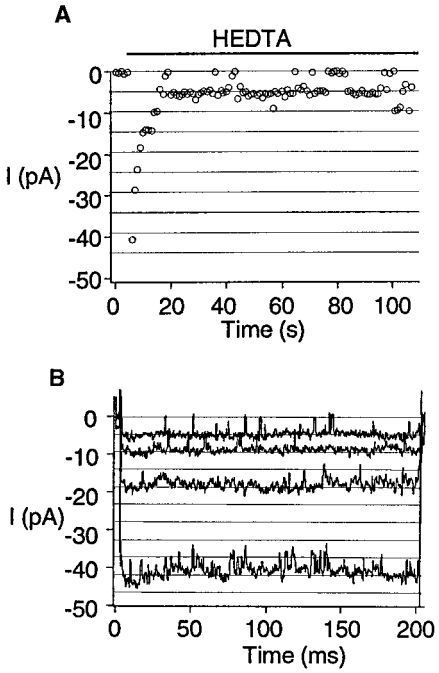


**Fig. 3.** Inactivation of $Na^+$ current through CRAC channels in single-channel steps, early in the activation of CRAC channels. Pipette solution contained $Mg^{2+}$. (**A**) External solution exchange from 20 mM $Ca^{2+}$ to $Na^+$ methane sulfonate containing HEDTA. (**B**) Representative current traces from the cell shown in (A).

the observed steps of current represent $Na^+$ current through single CRAC channels. $Ca^{2+}$, $Mg^{2+}$, $Ni^{2+}$, and $Gd^{3+}$, all of which inhibit current through CRAC channels, blocked the monovalent current detected from single channels (*9*). Single channels exhibited long-duration openings that were interrupted by rapid blocking and unblocking events when external $Mg^{2+}$ was buffered to 3 μM (Fig. 4, A to D). Blockade of channels by external $Mg^{2+}$ was voltage-dependent, as reflected in both the ensemble average of single-channel records and macroscopic *I-V* curves (Fig. 4, E and F).

We observed single-channel activity of a store-operated $Ca^{2+}$ channel as a succession of long-duration, independent single-channel events during activation of the macroscopic current. Macroscopic and single-channel $Na^+$ currents had the same reversal potential and *I-V* shape and were blocked by the same polyvalent cations. Extracellular $Mg^{2+}$ rapidly blocked and was released from the channel in discrete events, with concentration and voltage dependence similar to those of macroscopic currents, indicating a binding site deep within the electric field of the pore. With internal $Mg^{2+}$ present, inactivation of $Na^+$ current proceeded as single channels progressively closed. We conclude that the single-channel activity described reflects monovalent current through single CRAC channels. These observations support suggestions that CRAC is an ion channel and not a pump (*3–7*).

The single-channel conductance of 36 to 40 pS for the CRAC channel carrying $Na^+$ is 1500 times the estimated 24 fS for the $Ca^{2+}$ current through CRAC channels, but is close to the conductance of $Na^+$ through single L-type voltage-gated $Ca^{2+}$ channels (*11*). CRAC channels and voltage-gated $Ca^{2+}$ channels share several properties of ion permeation, including a common pore dimension of 6 Å and selectivity for $Ca^{2+}$ that depends on selective binding and interactions between $Ca^{2+}$ ions at the selectivity filter (*7, 12*). In both channel types, the smaller conductance of $Ca^{2+}$ compared to that of $Na^+$ results from a much higher affinity of $Ca^{2+}$ ions for the selectivity filter, which limits throughput but guarantees selectivity for the divalent ion.

From the measured macroscopic and single-channel currents and the average $P_o$,

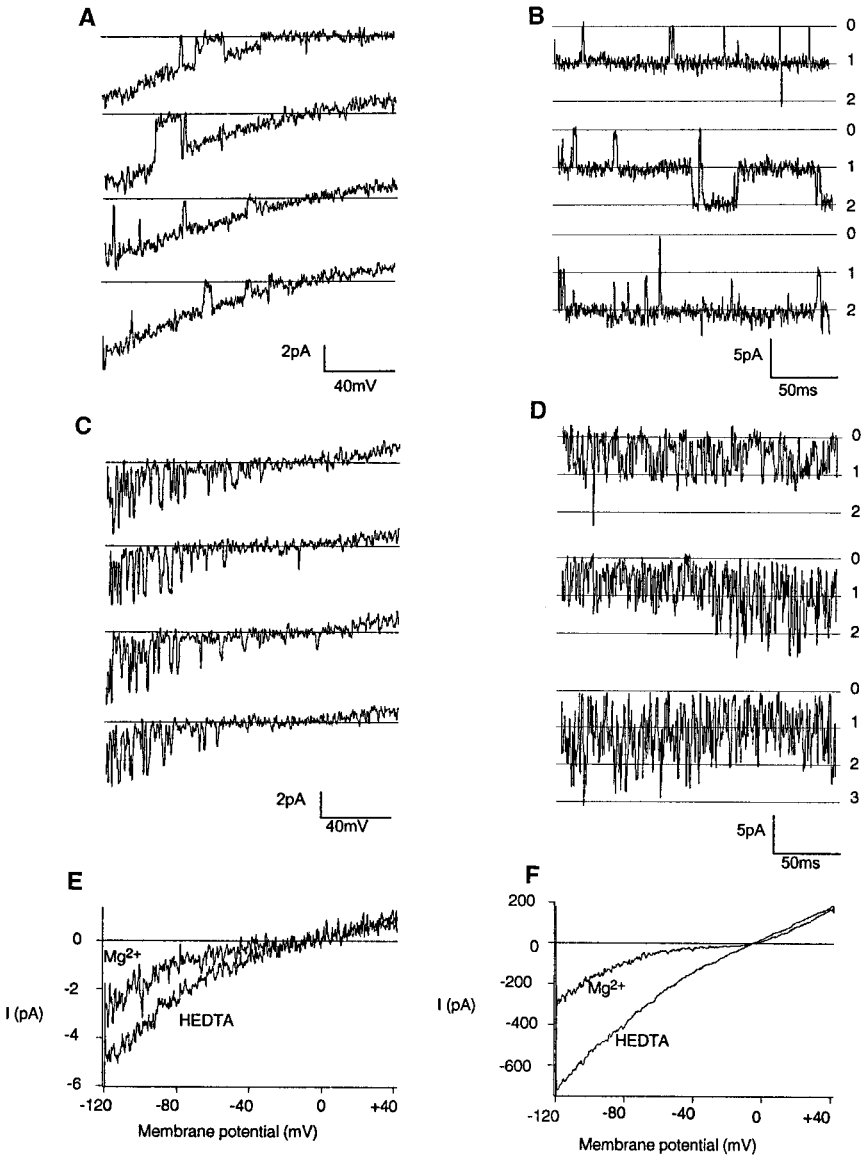


**Fig. 4.** Decrease in the open time and blockade of monovalent current in the presence of extracellular $Mg^{2+}$. External solution contained HEDTA; pipette solution was $Mg^{2+}$-free. (**A** and **B**) Single-channel activity during a voltage ramp from –120 to +40 mV and during 200-ms steps from 0 to –120 mV. (**C** and **D**) Block of single channels induced by buffering $Mg^{2+}$ to 3 μM. (**E**) Ensemble average of 12 current traces containing one ion channel with and without external 3 μM $Mg^{2+}$. Note the voltage-dependent block. (**F**) Macroscopic ramp current before and after addition of 3 μM $Mg^{2+}$. Currents were recorded from the same cell as shown in (A), (C), and (E), after complete activation of CRAC channels.

we conclude that there are 100 to 400 CRAC channels per cell, fewer than a previous estimate of more than 10,000 per cell derived from an analysis of conductance fluctuations (*13*). During the activation process, single CRAC channels opened abruptly and rapidly stabilized to a state of very high $P_o$, indicating an underlying mechanism that switches the single channels from a nonconducting state to a state in which $P_o$ is near unity. The identification of unitary CRAC channel currents provides a single-channel signature for identifying candidate genes and may facilitate the study of CRAC channel regulation.

### References and Notes


1. J. W. Putney, *Cell Calcium* **11**, 611 (1990); M. J. Berridge, *Biochem. J.* **312**, 1 (1995).
2. R. S. Lewis and M. D. Cahalan, *Annu. Rev. Immunol.* **13**, 623 (1995); M. D. Cahalan and K. G. Chandy, *Curr. Opin. Biotechnol.* **8**, 749 (1997).
3. R. S. Lewis and M. D. Cahalan, *Cell Regul.* **1**, 99 (1989); M. Hoth and R. Penner, *Nature* **355**, 353 (1992).
4. A. Zweifach and R. S. Lewis, *Proc. Natl. Acad. Sci. U.S.A.* **90**, 6295 (1993).
5. M. Hoth and R. Penner, *J. Physiol. (London)* **465**, 359 (1993).
6. A. Lepple-Wienhues and M. D. Cahalan, *Biophys. J.* **71**, 787 (1996).
7. H. H. Kerschbaum and M. D. Cahalan, *J. Gen. Physiol.* **111**, 521 (1998).
8. The human leukemic T cell line Jurkat E6-1 was cultured in RPMI 1640 with fetal calf serum (10%), 1 mM glutamine, and 25 mM Hepes in a 5% $CO_2$ incubator at 37°C. Cells were plated on polylysine-coated glass cover slips immediately before whole-cell recording with Sylgard-coated pipettes fire-polished to a resistance of 2 to 5 megohms. (Sylgard was purchased from Dow Corning; all other chemicals were from Sigma.) All experiments were done at room temperature (~20°C). Membrane currents were recorded with an EPC-9 patch clamp amplifier (HEKA, Lambrecht, Germany). Voltage stimuli lasting 200 ms were delivered from a holding potential of 0 mV every second, using either voltage ramps in which voltage increased from –120 to +40 mV or voltage steps from 0 to –120 mV. Currents were sampled at 5 kHz during voltage ramps and at 25 kHz during voltage steps. Currents were digitally filtered off-line at 1 kHz. CRAC channels were opened by passive depletion of $Ca^{2+}$ stores with 12 mM BAPTA or by addition of 10 μM $IP_3$, with ionic conditions chosen to eliminate currents through $K^+$ or $Cl^-$ channels. Traces recorded before the activation of CRAC channels were used as a template to subtract leak currents. Internal solutions contained 128 mM $Cs^+$ aspartate, 10 mM $Cs^+$-Hepes (pH 7.2), 12 mM BAPTA, 0.9 mM $CaCl_2$, and 3.16 mM $MgCl_2$. $Mg^{2+}$ was omitted from $Mg^{2+}$-free internal solution. Divalent-free external solution contained 150 mM $Na^+$ methane sulfonate, 10 mM *N*-hydroxyethyl-ethylenediamine-triacetic acid (HEDTA), and 10 mM Hepes (pH 7.2). The external $Ca^{2+}$ solution contained 20 mM $CaCl_2$ in addition to 120 mM $Na^+$ methane sulfonate. We added 370 μM $Mg^{2+}$ to 150 mM $Na^+$ methane sulfonate with 10 mM HEDTA to yield a calculated 3 μM free $Mg^{2+}$, as computed with Maxchelator [D. Bers, C. Patton, R. Nuccitelli, Eds., *A Practical Guide to the Study of $Ca^{2+}$ in Living Cells*, vol. 40 of *Methods in Cell Biology* (Academic Press, San Diego, CA, 1994)].
9. H. H. Kerschbaum and M. D. Cahalan, unpublished data.
10. Whole-cell $Na^+$ current densities after complete activation of CRAC channels averaged 153 ± 44 pA/pF with no $Mg^{2+}$ inside ($n$ = 45 cells) and 16 ± 6 pA/pF with internal $Mg^{2+}$ ($n$ = 10 cells).
11. P. Hess, J. B. Lansman, R. W. Tsien, *J. Gen. Physiol.* **88**, 293 (1986).
12. P. Hess and R. W. Tsien, *Nature* **309**, 453 (1984); E. W. McClesky and W. Almers, *Proc. Natl. Acad. Sci. U.S.A.* **82**, 7149 (1985); W. Almers, E. W. McClesky, P. T. Palade, *J. Physiol. (London)* **353**, 565 (1984).
13. Conductance fluctuation analysis is likely to have underestimated the single-channel conductance and overestimated the number of CRAC channels per cell, because the $P_o$ value of single channels is very high as soon as the CRAC channels begin to conduct. In stationary noise analysis, the single-channel conductance γ can be estimated by measuring the variance and mean conductance values ($\sigma_g^2$ and $G$) and then scaling according to the equation $\gamma = \sigma_g^2/[G(1 - P_o)]$. Using the value of $P_o$ = 0.94 determined here, a previous noise estimate of the single-channel $Na^+$ conductance of 2.6 pS can be corrected, resulting in a revised estimate of 43 pS, in good agreement with our direct single-channel measurements (*6*). If the same $P_o$ value also applies to high-divalent conditions, the variance and mean values of conductance estimated in (*4*) would correspond to a single-channel $Ca^{2+}$ conductance of ~400 fS. High-frequency block and unbinding by divalent ions above 1 kHz may also have lowered the variance and hence the single-channel $Ca^{2+}$ conductance estimated by noise analysis. An alternative approach to estimate the $Ca^{2+}$ conductance through a single CRAC channel is to divide the single-channel $Na^+$ conductance of 36 to 40 pS by the ratio of macroscopic $Na^+$ to $Ca^{2+}$ currents when divalents are withdrawn and then $Ca^{2+}$ reapplied, a ratio that averaged 25 (*7*). This approach assumes a constant number of open channels immediately before and after addition of $Ca^{2+}$ and yields an estimate of 1.6 pS for the CRAC channel carrying $Ca^{2+}$ at a concentration of 20 mM.


14. We thank L. Forrest for assistance in cell culture. Supported by NIH grants NS-14609 and GM-41514.

9 October 1998; accepted 11 January 1999